Eur. Phys. J. A **25**, 405–411 (2005)
DOI 10.1140/epja/i2005-10143-x

THE EUROPEAN PHYSICAL JOURNAL A

Molecular dynamics simulation for the baryon-quark phase transition at finite baryon density

Y. Akimura[1,2,a], T. Maruyama[2], N. Yoshinaga[1], and S. Chiba[2]

[1] Department of physics, Saitama University, 255 Shimo-Okubo, Sakura-Ku, Saitama City, Saitama 338-8570, Japan
[2] Advanced Science Research Center, Japan Atomic Energy Research Institute, Tokai, Ibaraki 319-1195, Japan

Received: 5 July 2005 / Revised version: 29 August 2005 /
Published online: 9 September 2005 –
Communicated by V. Vento

Abstract. We study the baryon-quark phase transition in the molecular dynamics (MD) of the quark degrees of freedom at finite baryon density. The baryon state at low baryon density, and the deconfined quark state at high baryon density are reproduced. We investigate the equations of state of matters with different *u*-*d*-*s* compositions. It is found that the baryon-quark transition is sensitive to the quark width.

PACS. 24.85.+p Quarks, gluons, and QCD in nuclei and nuclear processes – 12.38.Aw General properties of QCD (dynamics, confinement, etc.) – 12.39.Jh Nonrelativistic quark model – 21.65.+f Nuclear matter

1 Introduction

It is expected that quarks are observed as deconfined states in extreme environment: at high density and/or high temperature, where baryons or thermal pions overlap with each other, disappearance of hadron boundaries may give rise to the quark gluon plasma (QGP). Also the change of coupling constants and quark mass, due to the nature of quantum chromodynamics (QCD), is thought to be one of the origins of the QGP [1]. Recently, many theoretical calculations have been attempted to draw a QCD phase diagram [2–4]. The critical temperature of the hadron-quark phase transition is predicted to be around 150 MeV by lattice simulations [5,6]. For a finite-density system, the bag model predicts in a qualitative study [7] that the critical density lies at a few times the normal nuclear saturation density. Many efforts are devoted to the experimental search for the QGP by using high-energy accelerators. There, many indirect signals of the QGP have been observed [8–10] but a definite conclusion has not been obtained since theoretical studies are not enough to characterize the properties of the QGP and hadron gas at present. It is not clear how hadron matter changes to quark matter and how the physical properties change at the hadron-quark transition.

The lattice simulation based on the first principle is the most reliable method for QCD. It has been applied to high-temperature and low-density systems under some approximations. At high density, however, the complex fermion determinant, or the sign problem, makes the simulation practically impossible [11]. One of the approaches for treating finite-density systems is a mean-field theory which makes the most of its ability for uniform systems. There are many works with a mean-field treatment, which are incorporated with the chiral restoration by the Nambu–Jona-Lasinio model [12], the bag model picture [13], the soliton model picture [14], and so on. The dynamics of the hadron-quark transition, however, is not considered in these cases. In these circumstances, other approaches which are feasible for treating the finite density and the dynamics are being awaited.

Molecular dynamics (MD) has been successful in treating many-body nucleon systems. To describe the structure and the dynamics of many-body nucleon systems, several MD models were proposed [15–18] and some remarkable results have been obtained. Advantages of the MD simulation are that one needs very few assumptions *a priori* and that a single model can be applied to various problems. To investigate the properties of hadron and quark matter and the dynamics of the transition between these two phases in a unified manner, MD is a natural framework to be attempted. In this paper we apply a model similar to quantum molecular dynamics (QMD) [15] to many-body quark systems, within the framework of the nonrelativistic quark model. Some pioneering works on the application of MD to quark systems were presented where transitions caused by increasing density and temperature were studied from the viewpoint of many-body dynamics: in [19,20] the Vlasov equation and the Vlasov + MD approach were used to get the equation of state of matter. In [21] the quark MD was applied to heavy-ion collisions

[a] e-mail: akimura@phy.saitama-u.ac.jp

where the creation of particle-antiparticle pairs was taken into account. In [22], the color gauge symmetry was treated exactly and the meson exchange potentials were introduced. In the above studies quarks were treated as classical particles and there was ambiguity in the definition of the ground state of the system. In the present paper, we propose a model which has less ambiguity to describe the ground state (zero temperature). With this model we study the mechanism of the baryon-quark transition and draw the equation of state (EOS) for a wide range of baryon densities.

This paper is organized as follows. In sect. 2 we explain the basics of the model in detail. Simulation results for the three kinds of matters: *ud* (matter containing the same number of u and d quarks; it corresponds to symmetric nuclear matter), *udd* (d-quarks twice the number of u-quarks; neutron matter) and *uds* (the same number of u, d and s quarks; Λ matter) by using two kinds of quark width are given in sect. 3. The summary is given in sect. 4.

2 Molecular dynamics for quark matter

2.1 Wave functions and cooling equations

We start with the total wave function defined by a direct product of $n = 3A$ (A is the baryon number) single-particle quark Gaussian wave packets in the coordinate and momentum spaces and state vectors χ with a fixed flavor, a color and a spin orientation,

$$\Psi = \prod_{i=1}^{n} \frac{1}{(\pi L^2)^{3/4}} \exp\left[-\frac{(\mathbf{r}_i - \mathbf{R}_i)^2}{2L^2} + \frac{i}{\hbar}\mathbf{P}_i\mathbf{r}_i\right]\chi_i\,, \quad (1)$$

where L denotes the fixed width of wave packets, and $\mathbf{R}_i$ and $\mathbf{P}_i$ are the center of the wave packet of the i-th quark in the coordinate and momentum spaces, respectively. Instead of the antisymmetrization of the total wave function, the fermionic nature of the system is phenomenologically treated by introducing a Pauli potential which acts repulsively between quarks having the same flavor, color and spin orientation [23]. The equations of motion for $\mathbf{R}_i$ and $\mathbf{P}_i$ are given by the Newtonian equations,

$$\dot{\mathbf{R}}_i = \frac{\partial H}{\partial \mathbf{P}_i}, \qquad \dot{\mathbf{P}}_i = -\frac{\partial H}{\partial \mathbf{R}_i}, \quad (2)$$

where H denotes the effective Hamiltonian described later. When we search for the ground state (energy minimum configuration) of the system, we solve the equations of motion with friction terms, which we call "cooling equations of motion",

$$\dot{\mathbf{R}}_i = \frac{\partial H}{\partial \mathbf{P}_i} + \mu_r\frac{\partial H}{\partial \mathbf{R}_i}, \qquad \dot{\mathbf{P}}_i = -\frac{\partial H}{\partial \mathbf{R}_i} + \mu_p\frac{\partial H}{\partial \mathbf{P}_i}, \quad (3)$$

where μ_r and μ_p are negative frictional coefficients. The cooling is performed until the particles stop ($\dot{\mathbf{R}}_i = 0$). In the ground state, the momenta $\mathbf{P}_i$ have finite values because of the momentum dependence of the Pauli potential.

In order to simulate the infinite system (matter) by using a finite number of quarks, we use a cubic cell with 26 mirroring cells under a periodic boundary condition. The cell size is chosen to be 6 fm throughout this paper.

2.2 Effective Hamiltonian

The effective Hamiltonian consists of three parts as

$$H = H_0 + V_{\rm Pauli} - T_{\rm spur}, \quad (4)$$

where H_0 is the original Hamiltonian which contains a kinetic operator, color interaction and meson exchange potential acting between quarks,

$$H_0 \equiv \left\langle \Psi \left| \sum_{i=1}^{n} \hat{T}_i + \hat{V}_{\rm color} + \hat{V}_{\rm meson} \right| \Psi \right\rangle. \quad (5)$$

The expectation value of the kinetic operator is given by

$$E_i \equiv \left\langle \Psi \left| \hat{T}_i \right| \Psi \right\rangle = \frac{\mathbf{P}_i^2}{2m_i} + \frac{3\hbar^2}{4m_iL^2} + m_i. \quad (6)$$

We employ quark-quark interactions of the following forms:

$$\hat{V}_{\rm color} = \frac{1}{2}\sum_{i=1,j\neq i}^{n}\left(-\sum_{a=1}^{8}\frac{\lambda_i^a\lambda_j^a}{4}\left(K\hat{r}_{ij} - \frac{\alpha_s}{\hat{r}_{ij}}\right)\right), \quad (7)$$

$$\begin{aligned}\hat{V}_{\rm meson} = \sum_{i=1,i\in l}^{n}\Bigg[&\frac{1}{2-\varepsilon}\left(-\frac{g_{\sigma q}^2}{4\pi}\right)\left(\sum_{j\neq i,j\in l}^{n}\frac{e^{-\mu_\sigma\hat{r}_{ij}}}{\hat{r}_{ij}}\right)^{1-\varepsilon}\\ &+\frac{1}{2}\sum_{j\neq i,j\in l}^{n}\left(\frac{g_{\omega q}^2}{4\pi}\frac{e^{-\mu_\omega\hat{r}_{ij}}}{\hat{r}_{ij}} + \frac{\sigma_i^3\sigma_j^3}{4}\frac{g_{\rho q}^2}{4\pi}\frac{e^{-\mu_\rho\hat{r}_{ij}}}{\hat{r}_{ij}}\right)\Bigg]\\ &+\frac{1}{2}\sum_{i=1,i\in s}^{n}\sum_{j\neq i,j\in s}^{n}\frac{g_{\phi q}^2}{4\pi}\frac{e^{-\mu_\phi\hat{r}_{ij}}}{\hat{r}_{ij}}, \end{aligned} \quad (8)$$

where $\hat{r}_{ij} \equiv |\mathbf{r}_i - \mathbf{r}_j|$ and l means a light flavor, u or d.

The color-dependent interaction $\hat{V}_{\rm color}$ consists of the linear confining potential with an infrared cut-off at 3 fm and the one-gluon exchange potential [22] with the Gell-Mann matrices λ^a. To include the antisymmetric effect for the matrix elements of the color space, we use effective values $\langle\chi_i|\lambda_i^a\lambda_j^a|\chi_j\rangle^{\rm eff} = 4\langle\chi_i|\lambda_i^a\lambda_j^a|\chi_j\rangle$ [22]. The color force is approximately canceled between a colored quark and a white baryon made of quarks with three colors located near to each other. In previous works [24–26] a color magnetic interaction is used to reproduce the mass difference between the nucleon and the Δ to study finite systems. This interaction cannot be included in our model at present because the color- and spin-dependent interaction between baryons becomes too strong and causes unphysical behaviors even in the baryon phase.

The interaction $\hat{V}_{\rm meson}$ consists of σ-, ω- and ρ-meson exchange which act between light flavor quarks (u-quarks and d-quarks), and a ϕ-meson exchange potential which acts between s-quarks. In the ρ-meson exchange term, σ^3 indicates the third component of Pauli matrices for the isospin. We modify the σ exchange potential of Yukawa type with a small non-linearity parameter ε. This corresponds to a density-dependent potential or a non-linear σ term in the relativistic mean-field theory (RMF) where higher-order terms in the σ field are introduced to reproduce the saturation property of the symmetric nuclear matter. For simplicity, we have written eq. (8) in the form of an operator. In practice, however, the power by $1-\varepsilon$ of the σ exchange potential is performed after evaluating the expectation value. The parameters in the meson exchange potentials are adjusted to reproduce the baryon-baryon interactions as described in sect. 2.3.3.

The lack of antisymmetrization is compensated by using a Pauli potential,

$$V_{\rm Pauli} = \frac{C_p}{(q_0 p_0)^3} \exp\left[-\frac{(\mathbf{R}_i-\mathbf{R}_j)^2}{2q_0^2} - \frac{(\mathbf{P}_i-\mathbf{P}_j)^2}{2p_0^2}\right]\delta_{\chi_i\chi_j}, \tag{9}$$

where q_0, p_0 and C_p are parameters determined in sect. 2.3.2. Antisymmetrized wave functions are not used because it takes a CPU time proportional to the fourth power of the particle number [16,17]. On the other hand, MD without antisymmetrization requires CPU times proportional to the second power of the particle number. At present, simulation with antisymmetrization is not practically possible for a system with several hundreds of particles. Furthermore, the way to antisymmetrize wave functions with a periodic boundary condition has not been established yet.

We have to subtract the spurious zero-point energy of the center-of-mass motion of clusters [17,18],

$$T_{\rm spur} = \sum_{i=1}^{n} \frac{3\hbar^2}{4m_i L^2}\frac{1}{M_i}, \tag{10}$$

$$M_i \equiv \sum_{j=1}^{n} f_{ij}, \tag{11}$$

$$f_{ij} \equiv \begin{cases} 1\,, & (R_{ij} \le a_f)\,, \\ \exp\left[-\frac{(R_{ij}-a_f)^2}{w_f^2}\right], & (R_{ij} > a_f)\,, \end{cases} \tag{12}$$

where $R_{ij} \equiv |\mathbf{R}_i - \mathbf{R}_j|$ and M_i is the "mass number" of the fragment to which the wave packet i belongs, which is the sum of "friendship" f_{ij} with other particles. To apply the model to various densities, we introduce density-normalized parameters of cluster separation in the friendship as

$$a_f = a_0\left(\frac{\rho_0}{\rho}\right)^{1/3}, \qquad w_f = w_0\left(\frac{\rho_0}{\rho}\right)^{1/3}, \tag{13}$$

where ρ_0 means the normal nuclear density 0.17 fm^{-3}.

2.3 Choice of parameters

2.3.1 Quark model parameters and friendship

We use the constituent-quark mass $m_{u,d} = 300$ MeV for light quarks throughout this simulation. For the color potential, 900 MeV/fm is used for the string tension K and 1.25 for the QCD fine-structure constant α_s, which are typical of quark models [27].

The parameters in the friendship are chosen as $a_0 = 0.3$ fm and $w_0 = 0.5$ fm, so that the sum of the friendship $M_i \approx 3$ when the system clusterizes as baryons and $M_i \approx 1$ when quarks do not make clusters.

The width of the quarks L is the most important parameter in this model since it is directly related to the density at which the baryon-quark transition occurs. We use two different widths by considering the masses of the isolated nucleon N and the lambda particle Λ. To minimize the energy (mass) of a nucleon, L needs to be 0.43 fm. However, the nucleon mass is too large (about 2400 MeV) with this value of L. The reason of this overestimation is that the ground-state kinetic energy per quark in a nucleon, $\frac{2}{3}\frac{3\hbar^2}{4m_{u,d}L^2}$, has a large value of 351 MeV, while the kinetic energy of a quark in a nucleon is roughly estimated to be 50–80 MeV from the uncertainty principle. Therefore, we employ "effective" widths $L^{\rm eff}$ in evaluating E_i (eq. (6)) and $T_{\rm spur}$ (eq. (10)). The ground-state kinetic energy per quark in a nucleon becomes 65 MeV if we use $L^{\rm eff} = 1.0$ fm.

Our first choice is to use $L = 0.43$ fm, $L^{\rm eff}_{u,d} = 1.0$ fm. We call this choice as "parameter set (I)". This combination still gives a slightly large value of the nucleon mass, $M_N \approx 1500$ MeV. We select a strange-quark mass of 500 MeV which is often used in quark models. Then the difference of masses between N and Λ is reproduced by adjusting the effective width to be $L^{\rm eff}_s = 0.6$ fm.

Once the effective width $L^{\rm eff}$ for kinetic energy is employed, the nucleon mass does not have a minimum with respect to L. Then the second choice is made to give a proper nucleon mass value, $M_N \approx 940$ MeV, by changing L to be 0.33 fm (but with the same values of $L^{\rm eff}$ as before). Since the mass difference between N and Λ cannot be reproduced by adjusting the effective width in this case, we change the strange-quark mass to 567 MeV but the effective width for the s-quark is the same as for the u- and d-quark, $L^{\rm eff}_s = 1.0$ fm. We call this choice as "parameter set (II)".

2.3.2 Pauli potential

For the Pauli potential, the parameters C_p, q_0, p_0 are determined by fitting the kinetic energy to the exact Fermi gas at zero temperature. We determine these values by solving the cooling equations (3) for ud matter, udd matter and uds matter where only the Pauli potential is considered [23]. Figure 1 shows the classical and non-relativistic

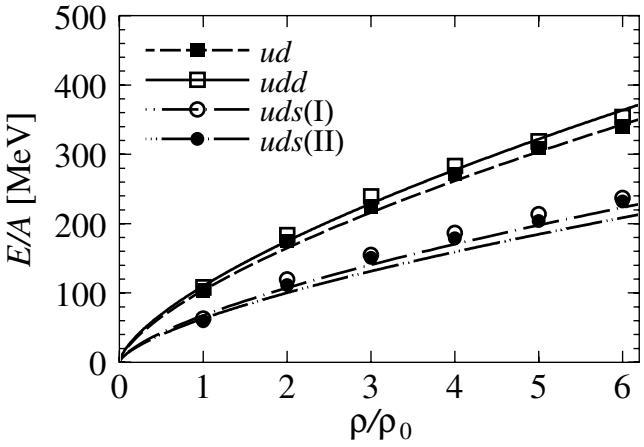

Fig. 1. Energy per baryon of the free Fermi gas. The lines show the theoretical exact values of *ud*, *udd* and *uds* matter. The marks are the kinetic energies calculated by MD with only the Pauli potential.

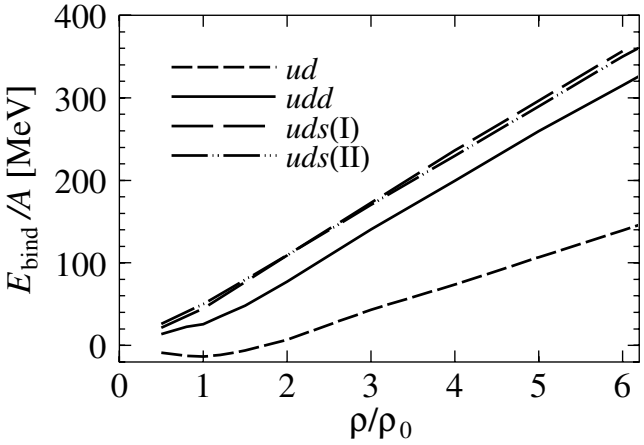

Fig. 2. Binding energies per baryon for *ud*, *udd* and *uds* matter calculated by the baryon cooling. The saturation is seen for the *ud* matter, but it is not seen for the *udd* and *uds* matter.

kinetic energy of the Fermi gas. The lines indicate the values of the exact Fermi gas energy for *ud* matter, *udd* matter and *uds* matter. The marks show the kinetic energy of each matter, whose values are obtained by using the following parameters: we adopt $q_0 = 1.6$ fm, $p_0 = 120$ MeV and $C_p = 131$ MeV for light quarks and $C_p = 79$ MeV for *s*-quarks. We use these parameters for both parameter sets (I) and (II) since the difference is slight. Here three different colors and two different spins are assumed for each matter. It is seen that the difference between *ud* matter and *udd* matter is small. By introducing heavy *s*-quarks, the Fermi energy of *uds* matter becomes lower than that of *ud* matter. Note that the Pauli potential gives a spurious potential energy to the system, which should be renormalized into other effective potential terms [23]. One possibility to avoid this problem is, instead of using the Pauli potential, to maintain the Pauli principle of the system by stochastic rearrangements of the particle momenta [28]. This model was originally developed for

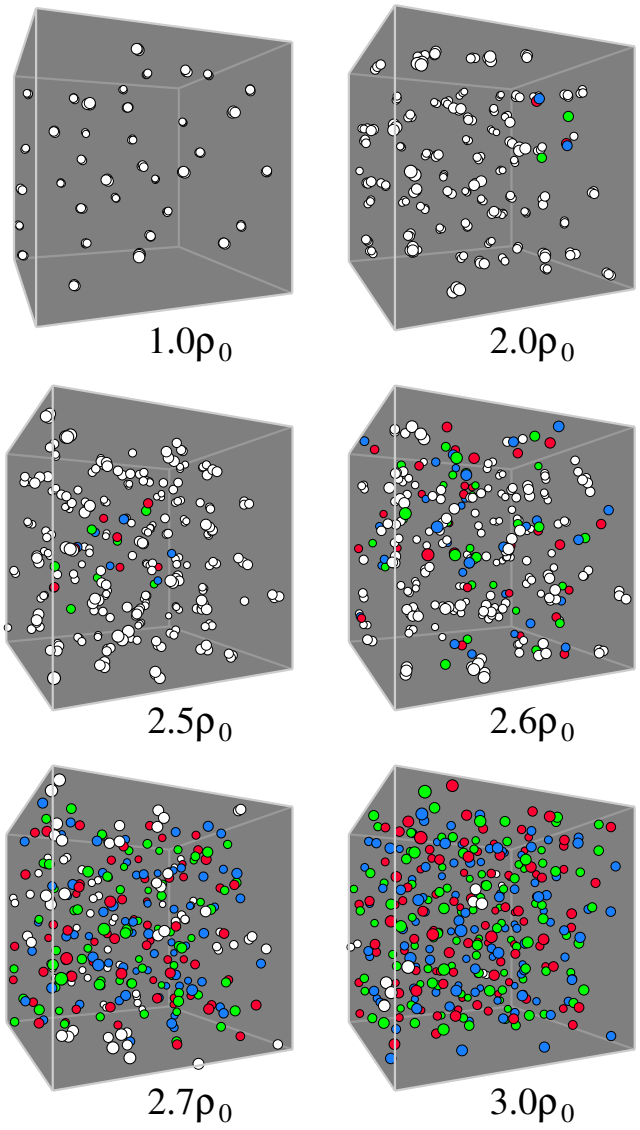

Fig. 3. Snapshots of *ud* matter with $L = 0.43$ fm at various densities. Using the criterion of eq. (15), confined quarks are plotted with white and deconfined quarks with their own color. At $1\rho_0$ all quarks are confined. As the density increases deconfined quarks or their colors begin to appear. Most of the quarks are deconfined at $3\rho_0$.

nucleon systems and was applied also to the quark system very recently [29].

2.3.3 Meson exchange potentials

Though the meson exchange potentials do not affect the baryon-quark transition, we adjust the meson exchange potentials to discuss the EOS of strange and normal nuclear matters. Prameters are determined to get the appropriate ground-state energy of "baryon matter" by frictional cooling with the constraint that quarks form baryon clusters (baryonization constraint). First, we randomly distribute baryons which are composed of three quarks

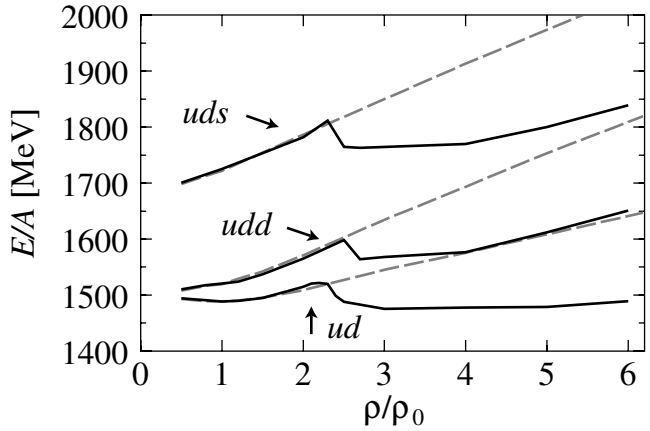

Fig. 4. Density dependence of energy per baryon for ud, udd and uds matter in case of parameter set (I) ($L = 0.43$ fm). The dashed lines indicate the cases of baryon cooling and solid lines quark cooling.

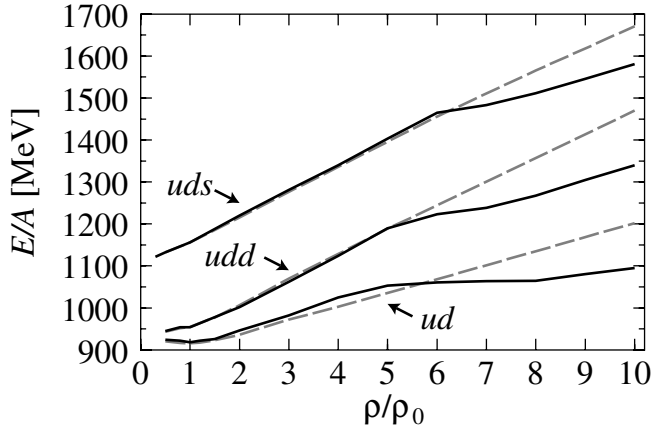

Fig. 5. Same as fig. 4, but with the parameter set (II) ($L = 0.33$ fm).

and solve the cooling equations with the baryonization constraint as

$$\dot{\mathbf{R}}_i = \frac{1}{3}\sum_{j\in\{i\}}\left[\frac{\partial H}{\partial \mathbf{P}_j} + \mu_r \frac{\partial H}{\partial \mathbf{R}_j}\right],$$
$$\dot{\mathbf{P}}_i = \frac{1}{3}\sum_{j\in\{i\}}\left[-\frac{\partial H}{\partial \mathbf{R}_j} + \mu_p \frac{\partial H}{\partial \mathbf{P}_j}\right]; \qquad (14)$$

here $\{i\}$ means a set of three quarks in a baryon to which the i-th quark belongs [22]. We call this cooling "baryon cooling". In fig. 2 the baryon density dependence of the energy per baryon is shown for ud matter, udd matter and uds matter. Note that in this calculation with the baryonization constraint, the color-dependent interactions are exactly canceled between the white baryons. For the σ exchange potential we use $g_{\sigma q} = 3.09$, $m_\sigma = 400$ MeV, $L_\sigma = 1.2$ fm and $\varepsilon = 0.1$, for the ω exchange potential $g_{\omega q} = 4.98$, $m_\omega = 782$ MeV and $L_\omega = 0.7$ fm, and for the ρ exchange potential $g_{\rho q} = 9.0$, $m_\rho = 770$ MeV and $L_\rho = 1.2$ fm. In order to reproduce the well-known properties of matter, we have introduced the effective widths L_σ, L_ω, L_ρ and L_ϕ for each meson exchange term. We fit the binding energy of ud matter to 16.5 MeV/nucleon at $1\rho_0$. The EOS of Λ matter, which depends on the ϕ exchange potential is unsettled yet [30]. In order to obtain the saturation of uds matter, we need to introduce an attractive K exchange interaction between u and s or d and s quarks. However, the K-meson exchange is prohibited according to the RMF model. Here we have only a repulsive ϕ exchange interaction between s-quarks for simplicity. The relevant parameters are $g_{\phi q} = \sqrt{2} g_{\omega q} = 7.04$ [30], $m_\phi = 1020$ MeV and $L_\phi = 0.7$ fm. Even if we use another value, *e.g.* $L_\phi \sim 1$ fm, the behavior of the EOS does not change noticeably.

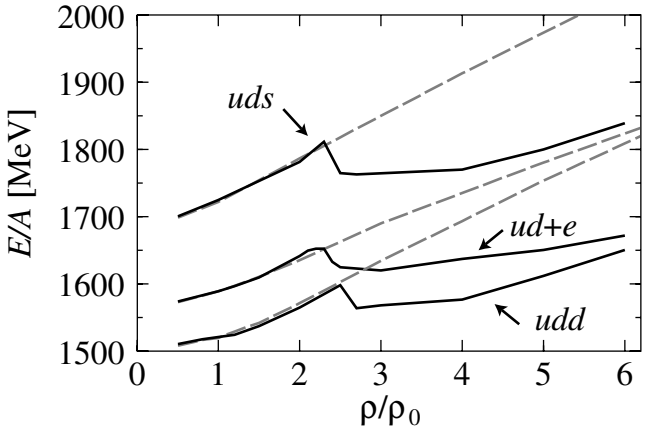

Fig. 6. Same as fig. 4, but under the electric charge-neutral condition.

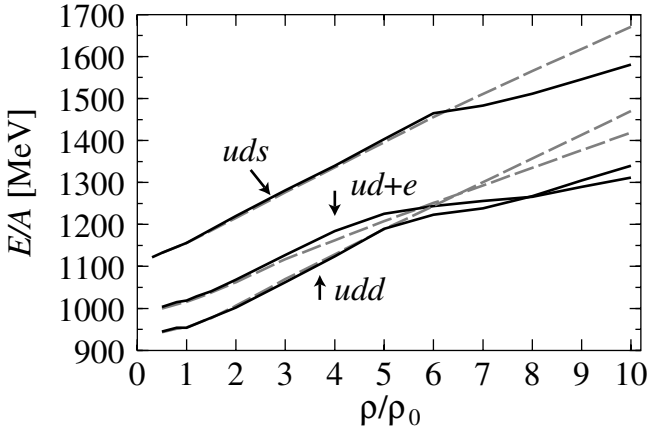

Fig. 7. Same as fig. 5, but under the electric charge-neutral condition.

3 Results for the finite-density system

Here we investigate stability and structure of quark matter in the ground state (zero temperature) for a wide range of densities. We solve the cooling equations (3) with quark degrees of freedom. We call this cooling "quark cooling" in contrast to the baryon cooling. Snapshots of

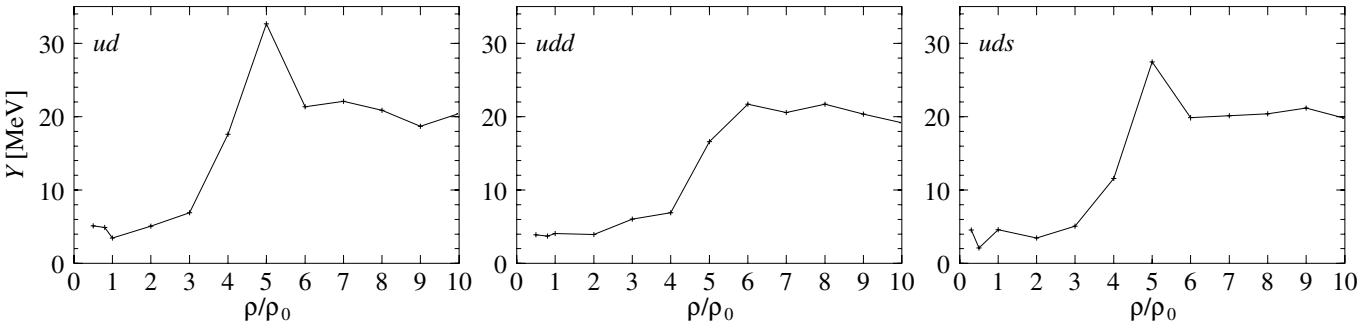

Fig. 8. Density dependence of Y defined by eq. (16) for ud, udd and uds matter in case of the parameter set (II) ($L = 0.33$ fm).

the ground state of ud matter with the parameter set (I) ($L = 0.43$ fm) are displayed in fig. 3. Three quarks in red, green and blue located within a distance $d_{\rm cluster}$ are considered to be confined as a baryon,

$$\begin{aligned} &|\mathbf{R}_i - \mathbf{R}_j| < d_{\rm cluster}, \\ &|\mathbf{R}_j - \mathbf{R}_k| < d_{\rm cluster}, \\ &|\mathbf{R}_k - \mathbf{R}_i| < d_{\rm cluster}, \\ &\quad \{i,j,k\} = \{\text{red}, \text{green}, \text{blue}\}, \end{aligned} \tag{15}$$

where we use $d_{\rm cluster} = 0.7$ fm. Quarks judged to be in a confined state are plotted in white and those deconfined in their own color. At the normal baryon density $1\rho_0$ all quarks are confined as baryons. As density increases, some quarks become deconfined and the confined and the deconfined states coexist around $2.5\rho_0$. Most of the quarks are deconfined at high baryon density $\rho \geq 3\rho_0$. The snapshots for the parameter set (II) look almost the same as for the parameter set (I) except for the value of the density. The ground-state energies of ud, udd and uds matters with the parameter set (I) are shown by solid lines in fig. 4. The vertical axis indicates the energy per baryon. For comparison, the case of baryon cooling is shown by thin dashed lines. The energy by quark cooling agrees with that by baryon cooling at low density. This means that quarks are confined as baryons. At a certain density, a baryon-quark transition occurs and the energy decreases. The mechanism of the baryon-quark transition in our dynamical model is as follows. If confined quarks are released from a baryon, their kinetic energy, most of which has been the zero-point energy, decreases. On the other hand, the potential energy increases due to the confinement force. Above a certain density, the increase of potential energy in deconfinement states gets smaller due to the existence of many other quarks in the environment. In this way, the decrease of the kinetic energy is superior to the increase of potential energy.

In our result with the parameter set (I), the critical density is lower than that usually expected. The ground-state energies by the parameter set (II) ($L = 0.33$ fm) are shown in fig. 5. The critical point of the baryon-quark transition is higher than that given by the parameter set (I). This implies that the transition occurs due to the density overlap of a quark with those in other baryons.

Figure 6 shows the energies for the three kinds of matters under the electric-charge neutral condition with the parameter set (I). The difference compared to fig. 4 is that the energy of the relativistic electron is added to the energy of ud matter. Below $6\rho_0$ the energy of udd matter is the lowest. Judging from the behavior of the curves, however, ud matter with the electron becomes more stable than udd matter above $6\rho_0$. Figure 7 shows the same quantity but for the parameter set (II). At $8\rho_0$ ud matter with the electron energy becomes more stable than udd matter.

The stability of strange matter has long attracted the interest of many nuclear and astro-physicists [31–33]. Our present result shows that uds matter is not favored even at high density. However, we cannot give a definite statement since our EOS of uds matter shows an ambiguity caused by the ignorance of the Λ-Λ interaction. The width of s-quarks and interactions concerning s-quarks influence the stability as well.

Here we have examined three kinds of fixed-flavor matter for simplicity. For more realistic studies of the matter realized in nature such as the core region of neutron stars, however, a simulation of matter in beta equilibrium is necessary. The most stable matter with non-integer u-d-s proportion would be close to udd matter at lower density, and between udd and ud matter at higher density. With the parameter set (I) there are density regions where the slope of E/A *versus* ρ/ρ_0 is negative in fig. 6. Generally such a situation is not realized by forming non-uniform structure. In our case, however, the small size of the simulation box and the introduction of density-dependent parameters (13) caused this problem. Therefore, we regard the results of the parameter set (I) as unrealistic.

Now, let us define a quantity Y which indicates the degree of deconfinement as

$$Y = \left(\left\langle \left| \sum_i^n V_{\rm color}\left(\mathbf{R}_i - \mathbf{R}\right) \right|^2 \right\rangle_{\mathbf{R}} \right)^{1/2}, \tag{16}$$

where $\mathbf{R}$ is the position of a test particle in any color, $V_{\rm color}$ is the color potential which the test particle feels and $\langle\rangle_{\mathbf{R}}$ means the average over $\mathbf{R}$ which is sampled for 10000 points. If all quarks are confined in compact baryons, the value of Y becomes zero. Figure 8 shows the density dependences of Y for the parameter set (II). The value of Y is small at low density. From $3\rho_0$ to $5\rho_0$ Y increases

gradually. This gradual change of Y does not necessarily indicate a second-order phase transition, since the mixed phase in the first-order phase transition may also show a similar behavior of physical quantities.

4 Summary

Many-body quark systems were studied by MD where the ground state was defined in a definite manner in terms of a Pauli potential. The EOSs were reproduced for three kinds of baryon matters with effective meson exchange interactions between quarks. The baryon-quark transition is seen when the baryon density increases. We have used two quark widths, $L = 0.43$ fm and $L = 0.33$ fm. The density at which the baryon-quark phase transition occurs is different for the two widths, since the transition is caused by the overlap of the quarks. In case of the larger value of $L = 0.43$ fm the baryon-quark transition occurs at rather low density, around $3\rho_0$. For the $L = 0.33$ fm case, the transition occurs around $5\rho_0$, which is consistent with other theoretical calculations.

We have compared three kinds of matters with different *u-d-s* compositions: *ud*, *udd* and *uds*. Our results show that the *ud* matter is the most stable among them at high baryon density and the strange *uds* matter is not stable. For the interaction and EOS of *uds* or Λ matter, there would be still room for improvement to take into account future experiments. For the color interaction, the color magnetic interaction is necessary as a color-, spin- and flavor-dependent interaction. The medium effects of constituent-quark masses by the chiral symmetry restoration are also important to discuss the stability. A possibility to include the medium effect is to use the density-dependent quark mass model (DDQM) [34]. However, the quark mass is derived there from the global density and is common for all quarks. This prescription may be too simple since the individual particle motion is essential in MD. A similar discussion can be done for the coupling constant α_s.

It is necessary to include the $\bar{q}q$ creation/annihilation process to extend this model to the finite-temperature systems. The lack of antisymmetrization is also an open problem.

Y.A. is grateful to T. Tanigawa, H. Koura, T. Tatsumi, T. Hatsuda, Y. Maezawa and T. Endo for their valuable discussions.

References

1. J.C. Collins, M.J. Perry, Phys. Rev. Lett. **34**, 1353 (1975).
2. T.M. Schwarz, S.P. Klevansky, G. Papp, Phys. Rev. C **60**, 055205 (1999).
3. J.B. Kogut, D.K. Sinclair, Phys. Rev. D **70**, 094501 (2004).
4. A. Tawfik, Phys. Rev. D **71**, 054502 (2004).
5. J.B. Kogut *et al.*, Phys. Rev. Lett. **51**, 869 (1983).
6. M. Stephanov, Prog. Theor. Phys. Suppl. **153**, 139 (2004).
7. H. Satz, Nucl. Phys. A **642**, 130 (1998).
8. M.C. Abreu *et al.*, Phys. Lett. B **477**, 28 (2000).
9. C. Adler *et al.*, Phys. Rev. Lett. **89**, 132301 (2002).
10. K. Suzuki *et al.*, Phys. Rev. Lett. **92**, 072302 (2004).
11. S. Ejiri, Phys. Rev. D **69**, 094506 (2004).
12. Y. Nambu, G. Jona-Lasinio, Phys. Rev. **122**, 345 (1961).
13. I.N. Mishustin, L.M. Satarov, H. Stöcker, W. Greiner, Phys. Rev. C **66**, 015202 (2002).
14. J. Berger, C.V. Christov, Nucl. Phys. A **609**, 537 (1996).
15. J. Aichelin, Phys. Rep. **202**, 233 (1991) and references therein.
16. H. Feldmeier, Nucl. Phys. A **515**, 147 (1990).
17. A. Ono, H. Horiuchi, T. Maruyama, A. Ohnishi, Prog. Theor. Phys. **87**, 1185 (1992).
18. T. Maruyama, K. Niita, A. Iwamoto, Phys. Rev. C **53**, 297 (1996).
19. A. Bonasera, Phys. Rev. C **60**, 065212 (1999).
20. A. Bonasera, Phys. Rev. C **62**, 052202 (2000).
21. M. Hofmann *et al.*, Phys. Lett. B **478**, 161 (2000).
22. T. Maruyama, T. Hatsuda, Phys. Rev. C **61**, 062201 (2000).
23. T. Maruyama, K. Niita, K. Oyamatsu, T. Maruyama, S. Chiba, A. Iwamoto, Phys. Rev. C **57**, 655 (1997).
24. A. De Rújula, H. Georgi, S.L. Glashow, Phys. Rev. D **12**, 147 (1975).
25. M. Oka, K. Yazaki, Prog. Theor. Phys. **66**, 556 (1981).
26. M. Oka, K. Yazaki, Prog. Theor. Phys. **66**, 572 (1981).
27. T. Yoshimoto, T. Sato, M. Arima, T.S.H. Lee, Phys. Rev. C **61**, 065203 (2000).
28. M. Papa, T. Maruyama, A. Bonasera, Phys. Rev. C **64**, 024612 (2001).
29. S. Terranova, A. Bonasera, Phys. Rev. C **70**, 024906 (2004).
30. H.Q. Song, R.K. Su, D.H. Lu, W.L. Qian, Phys. Rev. C **68**, 055201 (2003).
31. A.R. Bodmer, Phys. Rev. D **4**, 1601 (1971).
32. E. Witten, Phys. Rev. D **30**, 272 (1984).
33. N. Itoh, Prog. Theor. Phys. **44**, 291 (1970).
34. Z. Xiaoping, L. Xuewen, K. Miao, Y. Shuhua, Phys. Rev. C **70**, 015803 (2004).